

A Note on the "Various Atmospheres over Water Oceans on Terrestrial Planets" with a One-Dimensional Radiative-Convective Equilibrium Model

Tetsuya Hara* and Anna Suzuki†

Department of Physics, Kyoto Sangyo University, Kyoto 603-8555, Japan

Masayoshi Kiguchi‡

*Kindai University Research Institute for Science
and Technology, HigashiOsaka 577-8502, Japan*

Akika Nakamichi§

Institute of General Education, Kyoto Sangyo University, Kyoto 603-8555, Japan

Abstract

It has been investigated the possibility of the various atmospheres over water oceans. We have considered the H₂ atmosphere and He atmosphere concerning to N₂ atmosphere over oceans. One of the main subjects in astrobiology is to estimate the habitable zone. If there is an ocean on the planet with an atmosphere, there is an upper limit to the outgoing infrared radiation called the Komabayashi-Ingersoll limit (KI-limit). This limit depends on the components of the atmospheres. We have investigated this dependence under the simple model, using the one-dimensional gray radiative-convective equilibrium model adopted by Nakajima et al. (1992). The outgoing infrared radiation (F_{IRout}) with the surface temperature (T_s) has shown some peculiar behavior. The examples for H₂, He, and N₂ background gas for H₂O vapour are investigated. There is another limit called the Simpson-Nakajima limit (SN-limit) mainly composed of vapour. This steam limit does not depend on the background atmosphere components. Under super-Earth case ($g = 2 \times 9.8 \text{ m/s}^2$), several cases are also calculated. The KI-limit dependence on the initial pressure is presented. The various emission rates by Koll & Cronin (2019) are investigated.

Keywords: Hycean Worlds – Exoplanets atmospheres – H₂ atmospheres – He atmospheres – Komabayashi-Ingersoll limit – Simpson-Nakajima limit.

* hara@cc.kyoto-su.ac.jp

[†] i1785064@cc.kyoto-su.ac.jp

[‡] kiguchi-lab@abox3.so-net.ne.jp

[§] nakamichi@cc.kyoto-su.ac.jp

I. INTRODUCTION

It has been pointed that hydrogen could play an important role in the early stages of terrestrial planet history, when the disk gas is almost hydrogen and He at first (Sekiya, Nakazawa, & Hayashi 1981; Pierrehumbert & Gaidos 2011; Koll & Cronin 2019). It has been made-up word 'Hycean' referred to H₂ rich atmospheres over the massive oceans (Madhusudan et al. 2021). As hydrogen is light, it is said to escape to outer space (Sekiya, Nakazawa & Hayashi 1980), and it will take a long time to decrease to He dominant atmosphere (Hu et al. 2015).

Here we investigate cases of background gas with H₂ atmospheres over oceans. We also investigate cases with He atmospheres over oceans as well as N₂ atmospheres over oceans. It is taken the One-Dimensional Radiative-Convective Model adopted by Nakajima et al. (1992) for the gray atmosphere, which has been followed and investigated by many researchers (eg. Bressler & Shaviv 2015). The atmosphere is assumed to consist of the non-condensable component (mainly N₂, or H₂, He) and condensable component (eg. H₂O). For the stratosphere, radiative equilibrium is assumed. About the radiative transfer, the atmosphere is considered to be transparent to solar radiation in the optical range. In the infrared range, the absorption coefficient is taken to be constant and independent of wavelength which is said to be a gray atmosphere. The radiation transfer equation is integrated by using the Eddington approximation.

There are two important limits such as "Komabayashi-Ingersoll limit" (KI-limit; Komabayashi 1967; Ingersoll 1969) which is called "dilute limit" by Koll & Cronin (2019) and "Simpson-Nakajima limit" (SN-limit; Simpson 1927; Nakajima et al. 1992; Goldblatt et al. 2013) which is called "steam limit" by Koll & Cronin (2019). KI-limit is the upper limit for the emission from the top of the atmosphere in the Infrared radiation (F_{IRtop}) which depends on the component of the atmospheres and gravity.

SN-limit is the approximation limit of F_{IRtop} for H₂O atmosphere, which becomes the dominant component of the atmosphere in the high approximate temperature ($T \geq 500 \sim 600$ K), so it does not depend on the component of the background atmosphere. SN-limit depends only on the gravity in this paper for $\simeq 294$ W/m² for $g = 9.8$ m/s² and $\simeq 340$ W/m² for $g = 2 \times 9.8$ m/s², respectively.

For H₂ background atmospheres, it is characteristic that F_{IRtop} increases with surface

temperature T_s at the first time, however, it seems to reach the upper limit, then decrease down and again increase to reach the second saturated limit denoted as the SN-limit (Goldblatt & Watson 2012). This feature is noticed by Suzuki (2017) and is named as "Soufflé Effect" by Koll & Cronin (2019). One of the purpose of this work is to investigate the various limits and mechanism of these features.

We calculate cases of the surface accelerating gravity $g=9.8 \text{ m/s}^2$ and $2 \times 9.8 \text{ m/s}^2$. The latter corresponds to almost ten times of Earth mass, called super-Earth (Madhusudhan et al. 2021). Although it is pointed out that molecular hydrogen interacts strongly with infrared radiation via collision-induced absorption (CIA) in the high pressure situation (Wordsworth & Pierrehumbert 2013), we have not considered such effects for H_2 and N_2 here. We assume that background gases except H_2O are transparent.

The only assumed different part among H_2 , He and N_2 is the mean molecular weight \bar{m} of the background gas, given by

$$\tilde{m} = m_n x_n + m_v x_v. \quad (1)$$

The parameter m_n and m_v are the molecular (or atomic) weight of the non-condensable and condensable (vapour) components, respectively. And the parameters x_n and x_v are the mole fractions of the non-condensable and condensable components, respectively.

In Sect. II, the method of the model is outlined. It is applied to H_2 atmosphere in Sect. III and applied to He atmosphere in Sect. IV. In Sect. V, the KI-limit dependence on the initial pressure is investigated. The results and discussion are deployed in Sect VI..

II. ONE-DIMENSIONAL RADIATIVE-CONVECTIVE MODEL

We have followed the method of Nakajima et al. (1992) for the One-Dimensional Radiative-Convective Model. Under the tropopause, the adiabatic lapse rate is adopted where water vapour is saturated. It is assumed that the saturation water vapour pressure p^* is derived under the Clausius-Clapeyron relationship and given by

$$p^*(T) = p_o^* \exp\left(-\frac{l}{RT}\right), \quad (2)$$

where T and R are temperature, the gas constant, respectively. The l , and p_o^* are the latent heat of condensable component ($l = 43655 \text{ J mol}^{-1}$), and the constant for water saturation curve ($p_o^* = 1.4 \times 10^{11} \text{ Pa}$).

For the troposphere, it is assumed to be pseudoadiabatic lapse rate for the temperature gradient with pressure as

$$\left(\frac{\partial T}{\partial p}\right) = \frac{\frac{RT}{pc_{pn}} + \frac{x_v^* l}{x_n pc_{pn}}}{x_n + x_v^* \frac{c_{pv}}{c_{pn}} + \frac{x_v^* l^2}{x_n RT^2 c_{pn}}}, \quad (3)$$

where c_{pv} , and c_{pn} are the mole specific heat at constant pressure of condensable and non-condensable components, respectively.

Nakajima et al. have assumed that the molecular weights are the same for condensible and non-condensable substances for simplicity. It is checked that the above equation (3) is applicable to the different molecular weights and the derivation of the above equation is commented in Appendix A.

Given the non-condensable pressure p_{n0} and temperature at the surface T_s , $T(p)$ is obtained up to the tropopause of the atmosphere. There appears to be a height where the net convergence becomes positive in the upper levels of the atmosphere. The position of the tropopause is taken to be there.

A. Upper limit (KI-limit)

One of the main problems in astrobiology is to find out the habitable zone where liquid water could exist. The injection from the central emitting object (Sun) increases when the planet comes near to the center. On the other hand, there is an upper limit that the planet could emit radiation. It depends on the atmospheric component and this paper investigates of the dependence under a simple model.

The optical depth τ is defined as

$$\tau = \int_z^\infty \kappa \rho dz. \quad (4)$$

The only assumed different part of H₂ and He from N₂ is the mean molecular weight of the background gas. The different point is the following equation about the optical depth τ (Nakajima et al. 1992)

$$d\tau = (\kappa_v x_v m_v + \kappa_n x_n m_n) \frac{dp}{\bar{m}g}, \quad (5)$$

where p is the pressure and g is the acceleration of gravity. As we assume $\kappa_n = 0$, the effective factor $\bar{m}/(x_v m_v)$ for gravity has changed due to the mole fraction, and mean molecular weight.

In the stratosphere where T and x_n are almost constant, the integration of Eq. (5) becomes

$$\tau = (\kappa_v x_v m_v + \kappa_n x_n m_n) \frac{p}{\bar{m}g}. \quad (6)$$

The stratosphere is in a radiative equilibrium and the temperature structure is given as

$$\pi B = \frac{1}{2} F_{IRtop} \left(1 + \frac{3}{2} \tau \right), \quad (7)$$

where $B = \sigma T^4 / \pi$ is the blackbody radiation intensity. At the tropopause, we have

$$\frac{1}{2} F_{IRtop} \left(1 + \frac{3}{2} \tau_{tp} \right) = \sigma T_{tp}^4, \quad (8)$$

and

$$\tau_{tp} = \kappa_v p^*(T_{tp}) \frac{1}{g} \frac{m_v}{\bar{m}}. \quad (9)$$

There is a maximum value of F_{IRtop} ($= F_{KI-limit}$) which will satisfy the above two equations which is denoted Komabayashi-Ingersoll limit (Nakajima et al. 1992).

III. APPLIED TO H₂ BACKGROUND ATMOSPHERE

It is investigated the gray calculations for cases of background gases with H₂ for $g = 9.8\text{m/s}^2$. The relationships between T_s and F_{IRtop} for several initial $p_{H_2,0}$ cases are presented in Fig. 1.

For H₂ background atmosphere, it is characteristic that F_{IRtop} increases with surface temperature T_s at the first time, however, it seems to reach the upper limit, then decrease down and again increase to reach the second saturated limit denoted as the SN-limit (Goldblatt & Watson 2012).

The first upper limit is due to the dominant H₂ background atmosphere, where the optical depth is unity at the gas temperature $T \simeq 260 \sim 280$ K as shown in Figs. 2 and 3 where the case of $P_{H_2,0} = 10^6$ Pa is presented. The decrease of F_{IRtop} after the first upper limit is due to the temperature decrease of the gas temperature corresponding to the region where the optical depth is about unity (later we call it as unity optical depth). After the lower limit of F_{IRtop} , it increases due to the temperature increase of the gas temperature corresponding to the unity optical depth which is shown in Fig. 2 and magnified in Fig. 3, where the detailed feature could be seen. The F_{IRtop} then increases to the SN-limit as shown in Fig. 1.

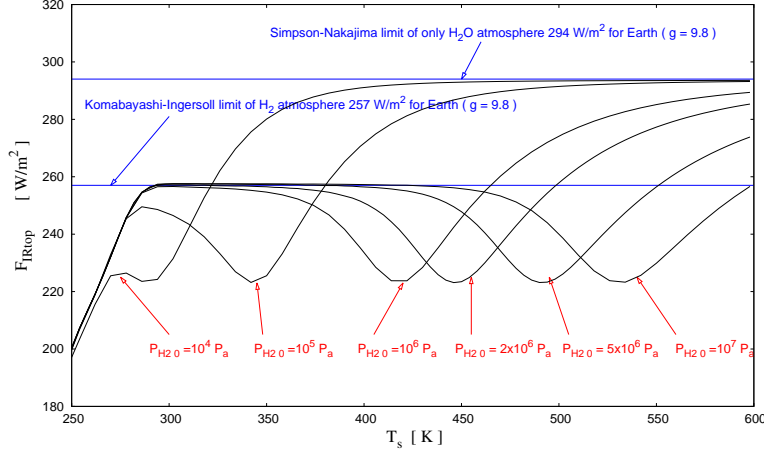


FIG. 1. The relationships between T_s and F_{IRtop} for several initial p_{H_2O} ($= 10^4, 10^5, 10^6, 2 \times 10^6, 5 \times 10^6$, and 10^7 Pa) cases of H_2 .

A. Moist tropospheric asymptotic limit (SN-limit)

There is a limit of F_{IRtop} that the initial p_0 of the background atmosphere is small or null where the atmosphere is consisted almost only of saturated H_2O vapour. This is called the "Moist tropospheric asymptotic limit", "Saturated vapour limit", "SN-limit" (Goldblatt & Watson 2012), or "steam limit" (Koll & Cronin 2019). The second upper limit is the same with the only water vapour atmosphere, being the case of saturated vapour pressure ($\simeq 294$ W/m^2 for $g = 9.8m/s^2$ and $\simeq 340$ W/m^2 for super-Earth in Fig. 10).

When the surface temperature is enough high, the mole fraction of water vapour is almost unity and optical depth increases. When the optical depth is smaller than unity, the outgoing flux comes from the bottom of the Hydrogen atmosphere. However, when optical depth is greater than unity, the outgoing flux comes from the place where the optical depth is almost unity from the top of the atmosphere (UOD: unity optical depth). Then the outgoing flux is almost the same as that of a pure H_2O atmosphere.

The relationships between surface temperature T_s and optical depth (τ) of $p_{H_2O} = 10^6$ Pa for several T_s cases are presented in Fig. 2. The cases of $T_s = 250K, 300K, 350K, 400K, 450K, 500K, 550K,$ and $600K$ are presented by red, dark-red, brown, orange, purple, light-blue, blue, and green colour curve, respectively, The unit optical depth ($\tau = 1$) is also presented by the red line and the magnified figure is presented in Fig. 3.

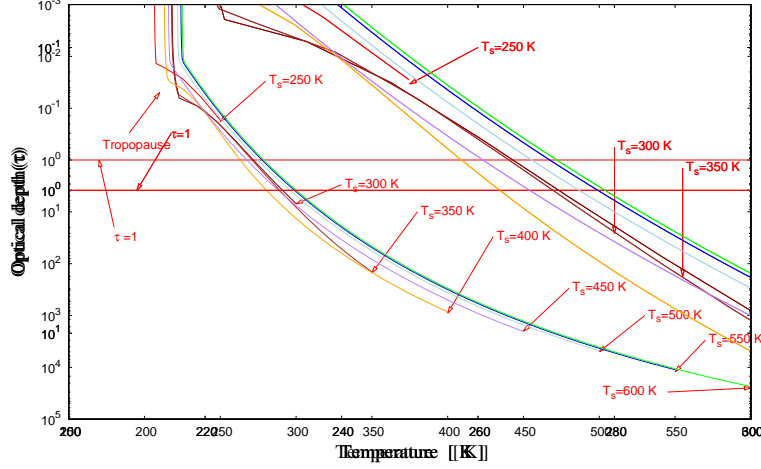


FIG. 2. The relationships between T_s and optical depth (τ) of $p_{H_2O} = 10^6$ Pa for several T_s cases.

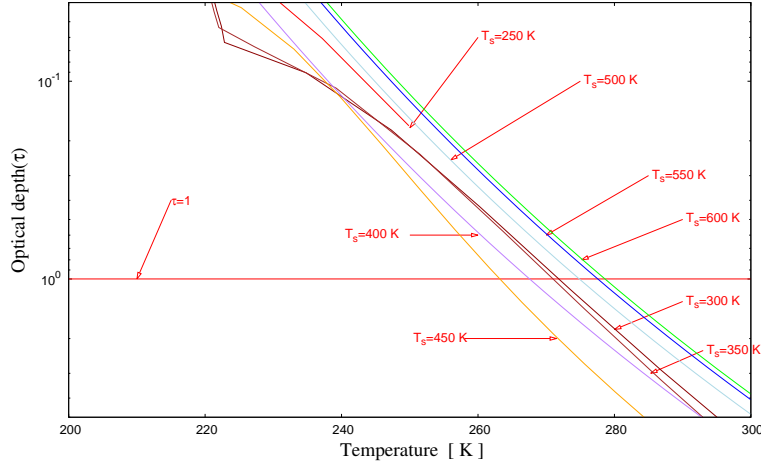


FIG. 3. The relationships between T_s and optical depth (τ) of $p_{H_2O} = 10^6$ Pa for several T_s cases are presented. It is the magnified figure of Fig. 2 to explain the change of F_{IRtop} for different of T_s .

The luminosity is mainly radiated at around $\tau \simeq 1$ and the intensity is related to the local temperature of $\tau \simeq 1$. The first bump of $p_{H_2O} = 10^6$ in Fig. 1 is appeared at $T_s = 300 \sim 350$ K and then the luminosity decreases around $T_s = 400 \sim 450$ K and then increases around $T_s = 500 \sim 600$ K. The detailed features could be seen in Fig. 3 as the line of $\tau = 1$ is crossed by each T_s curve.

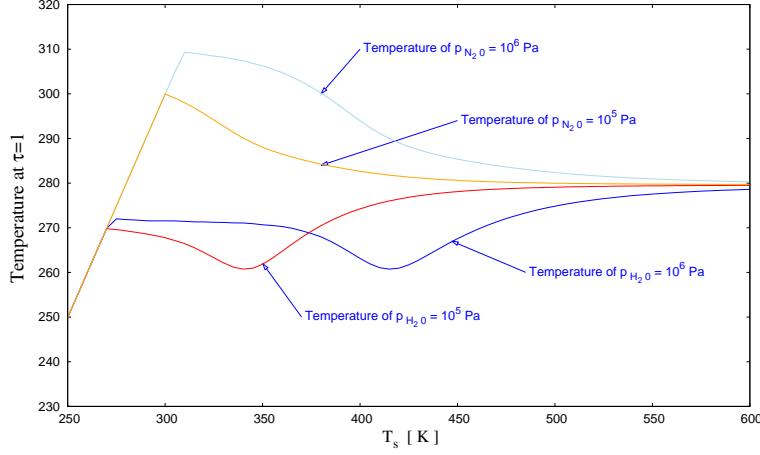


FIG. 4. The relationships between the temperature of UOD (Unity optical depth) and T_s of $p_{H_2O} = 10^6$ and 10^5 Pa are presented by blue and red curves, respectively. The cases for N_2 atmospheres of $p_{N_2O} = 10^6$ and 10^5 Pa are also presented for reference by light blue and orange curves, respectively.

The features could be understood in Fig. 4, where the relationship between the temperature at UOD (Unity optical depth) and T_s of $p_{H_2O} = 10^6$ Pa is presented by blue curves. The luminosity decreases around $T_s = 400 \sim 450$ K and then increases around $T_s = 500 \sim 600$ K. The case of $p_{H_2O} = 10^5$ Pa is shown there by red curve. The cases for N_2 atmospheres of $p_{N_2O} = 10^6$ and 10^5 Pa are also presented for reference by light blue and orange curves, respectively. For the case that the total optical depth is smaller than unity, the temperature of UOD is assumed to be equal to T_s .

In Fig. 5, the relationships between the height of UOD and T_s of $p_{H_2O} = 10^6$ is presented by blue and curve. The height of UOD has increased to ~ 350 km, where the temperature of UOD has decreased to ~ 260 K (see Fig. 4). The case of $p_{H_2O} = 10^5$ Pa is shown there by red curve. The cases for N_2 atmospheres of $p_{N_2O} = 10^6$ and 10^5 Pa are also presented for reference by light blue and orange curves, respectively. The height of UOD is taken to be zero for the case that the total optical depth is smaller than unity.

In the low temperature limit, the lapse rate is assumed to be the dry adiabat, $dT/dz = -g/c_p$, as described in Pierrehumbert (2010) and Appendix B

$$H_T^{dilute} = \frac{c_p T}{g} \propto 1/M, \quad (10)$$

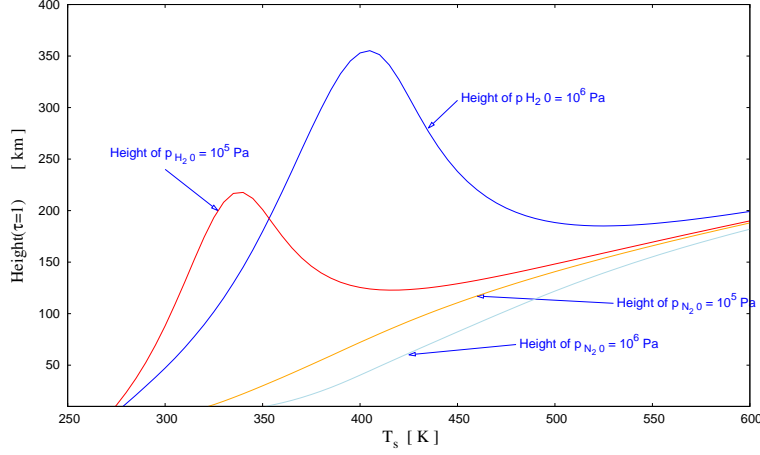


FIG. 5. The relationships between the height of UOD and T_s of $p_{H_2O} = 10^6$ and 10^5 Pa are presented by blue and red curves, respectively. The cases for N_2 atmospheres of $p_{N_2O} = 10^6$ and 10^5 Pa are also presented for reference by light blue and orange curves, respectively. The height is zero for the case that the total optical depth is smaller than unity.

where c_p is the specific heat per unit mass and proportional to the inverse of the molecular weight M . In Appendix B, it is investigated the analytical expression derived by Koll & Cronin (2019) for the OLR limit values of the steam limit and dilute limit. In Appendix C, it is tried to derive Eq. (33) in Koll & Cronin (2019) for suspected typos.

It should be noted that at $T_s \sim 400$ K for $p_{H_2O} = 10^6$ Pa the height of UOD has increased to $H_T^{UOD} \simeq 350$ km in H_2 , whereas $H_T^{UOD} \simeq 40$ km in N_2 . The main difference must be due to the low molecular weight of H_2 relative to N_2 .

The increase of the UOD height is related to the features that F_{IRtop} increases with surface temperature T_s at first time then decreases down and again increase to reach the second saturated limit. The first F_{IRtop} increase is due to the increase of T_s and the lower value of the water vapour (Figs. 6 and 7). The F_{IRtop} upper limit is due to the KI-limit. The F_{IRtop} decrease is due to the increase of the water vapour and the optical depth (Figs. 6, 7, and 8). The UOD height increase is related to the decrease the UOD temperature (Figs. 4 and 5). The second saturated limit is due to the increase and saturation limit of the water vapour (Figs. 4 ~8).

The relationships between temperature and pressure of $p_{H_2O} = 10^6$ Pa for several T_s

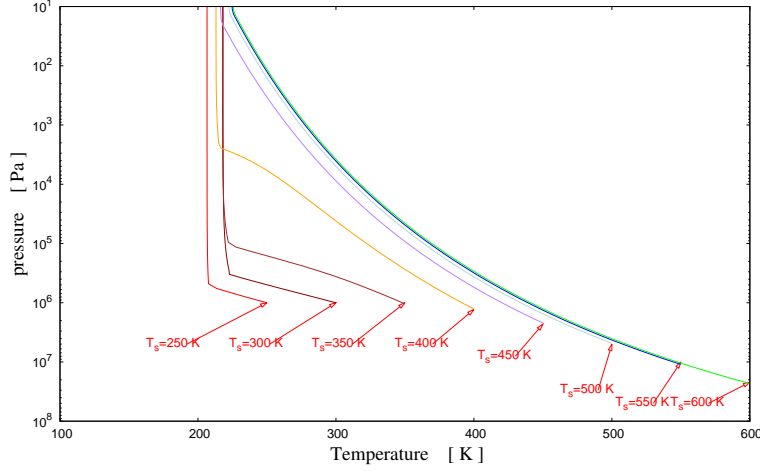


FIG. 6. The relationships between temperature and pressure for several T_s cases of $p_{H_2 0} = 10^6$ Pa.

cases are calculated in Fig. 6 and the relationships between mole fraction and pressure are shown in Fig. 7. In Fig. 8, the relationships between mole fraction and optical depth are presented.

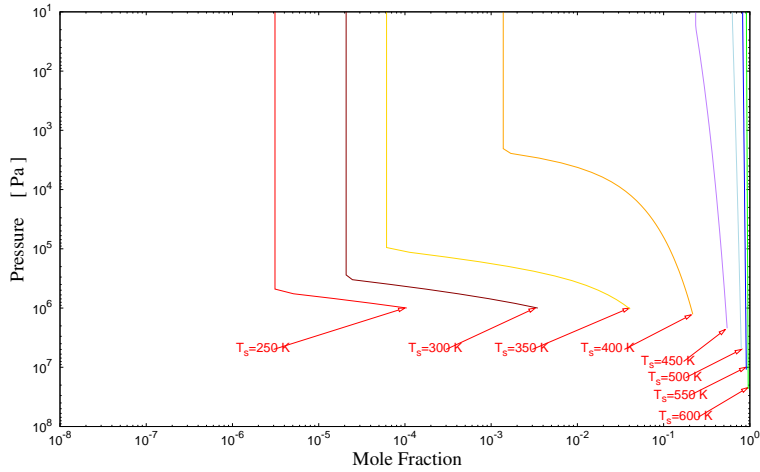


FIG. 7. The relationships between the mole fraction of the water vapour and the pressure of $p_{H_2 0} = 10^6$ Pa for several T_s cases.

For H_2 atmosphere, optical depth τ at tropopause is given by Eq. (9) where the factor m_v/\bar{m} increases about 10 from N_2 to H_2 atmosphere which causes the decrease of KI-limit

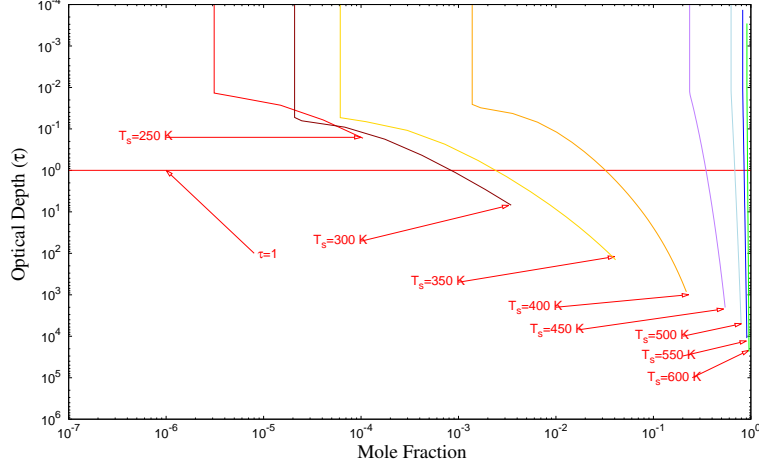


FIG. 8. The relationships between the mole fraction and the optical depth for several T_s cases of $p_{H_2, 0} = 10^6$ Pa.

($\simeq 420$ W/m² (N₂) to $\simeq 257$ W/m² (H₂), as shown in Fig. 9).

The difference between N₂ and H₂ background atmosphere is the difference of the mean molecular weight which corresponds to the change of the optical depth. For H₂ atmosphere, the optical depth has increased. Even for the same surface temperature, the temperature at optical depth $\tau = 1$ decreases for H₂ atmosphere. Then the outgoing radiation has decreased for the H₂ atmosphere compared to the N₂ atmosphere.

If H₂ pressure increases, the outline of the graph has moved to the right-hand which is shown in Fig. 1. If the surface temperature increased to the right-hand direction, there is a possibility that the ocean would evaporate.

The relationships between T_s and F_{IRtop} for several $p_{H_2, 0}$ and $p_{N_2, 0}$ cases are presented in Fig. 9. Some H₂ results in Fig. 1 are included in Fig. 9. The cases of N₂ are almost the same given in Nakajima et al. 1992, except that the molecular weight of N₂ is taken 28 (it is taken 18 in Nakajima et al. (1992) for its simplicity), then KI-limit has increased from $\simeq 385$ W/m² to $\simeq 420$ W/m².

The cases of H₂ for super-Earth ($g = 9.8 \times 2$ m/s²) are shown in Fig. 10.

In Fig. 11, super-Earth cases of background gases with H₂ and N₂ are presented for the relationships between T_s and F_{IRtop} in several initial $p_{H_2, 0}$ cases. The arrow of P_{H_2O} shows the case of $p_{H_2, 0} = 0$ Pa which means only H₂O atmosphere component corresponding to

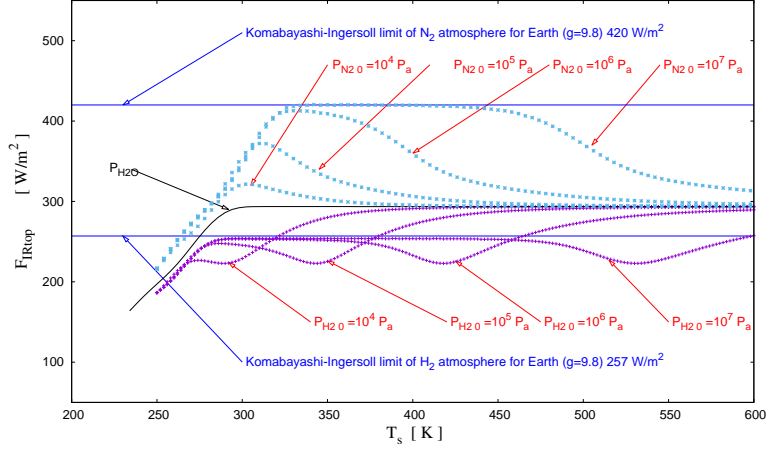


FIG. 9. It is compared the gray calculations for cases of background gases with H_2 and N_2 for $g = 9.8m/s^2$. The relationships between T_s and F_{IRtop} for several initial $p_{H_2,0}$ and $p_{N_2,0}$ cases are presented. Some H_2 results in Fig. 1 are included. The arrow of P_{H_2O} shows the pure H_2O case and SN-limit ($\simeq 295 W/m^2$).

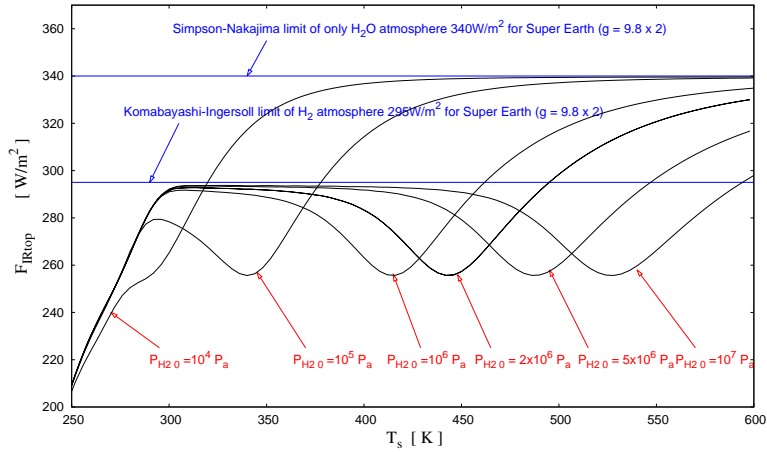


FIG. 10. For super-Earth cases with H_2 atmosphere, the relationships between T_s and F_{IRtop} for several initial $p_{H_2,0}$ cases are presented.

the SN-limit.

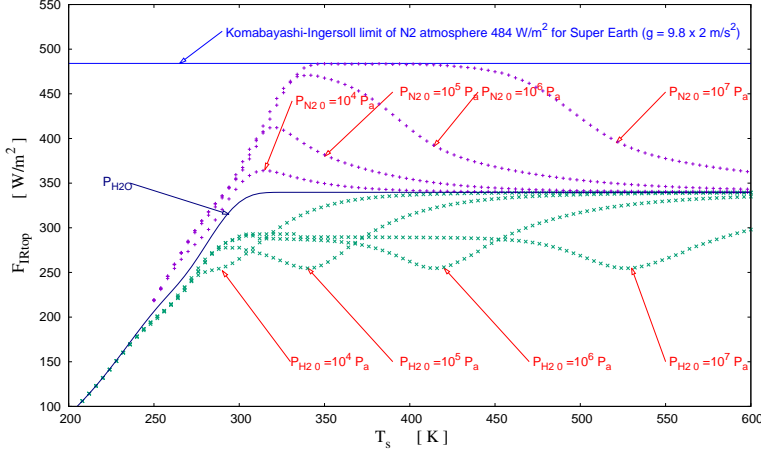


FIG. 11. For super-Earth cases of background gases with H_2 and N_2 , the relationships between T_s and F_{IRtop} in several initial $p_{\text{H}_2,0}$ cases are presented. The arrow of $P_{\text{H}_2\text{O}}$ shows the case of $p_{\text{H}_2,0} = 0$ Pa which means only H_2O atmosphere component corresponding to SN-limit.

IV. APPLIED TO He BACKGROUND ATMOSPHERE

The situations of He background atmosphere are similar to the case of H_2 background atmosphere except the treatment of the mean molecular weight and the specific heat of He as $c_p = 2.5 R$, being mono atomic gas, compared to that of H_2 , as $c_p = 3.5 R$, being dipole atomic gas.

In Fig. 12, the results of He atmosphere are similar to those of H_2 cases in Fig. 1. The first upper limit of $p_{\text{He},0} = 10^6$ and 10^7 are the KI-limit of He atmosphere. Then they decrease down and increase approximately to the SN-limit as the cases of H_2 background gas as presented in Fig. 1.

It must be noticed that the KI-limit for He atmosphere is $\simeq 291 \text{ W/m}^2$ which is almost the same value of the SN-limit $\simeq 294 \text{ W/m}^2$. It seems to be a problem that the SN-limit is greater than the KI-limit, however it is not a problem because the components of the background atmospheres have changed from He to H_2O . It is almost the same for H_2 atmosphere cases in Fig. 1.

It is pointed out by Koll & Cronin (2019) that H_2 is the only background gas for which the dilute runaway (KI-limit) lies below the steam limit (SN-limit). However as shown in Fig 12, He is also the background gas for which the dilute limit lies below the steam limit.

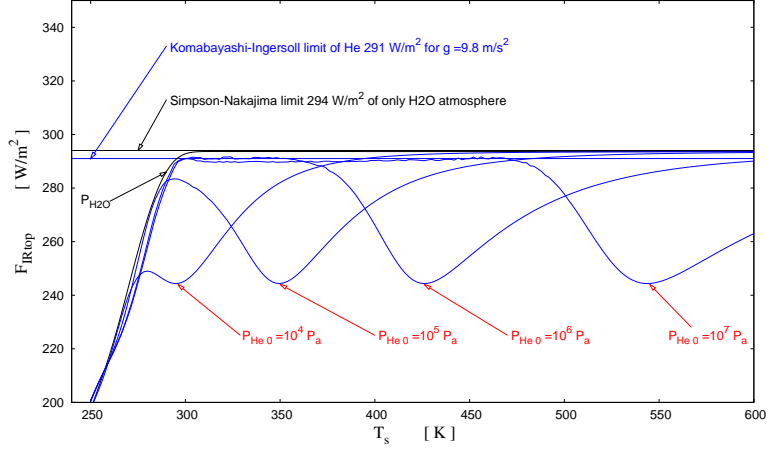


FIG. 12. For He background gases of $g = 9.8\text{m/s}^2$, the relationships between T_s and F_{IRtop} for several initial $p_{He\ 0}$ cases are presented. The value of KI-limit for He atmosphere is $\simeq 291\text{ W/m}^2$ which is almost the same value of the SN-limit $\simeq 294\text{ W/m}^2$.

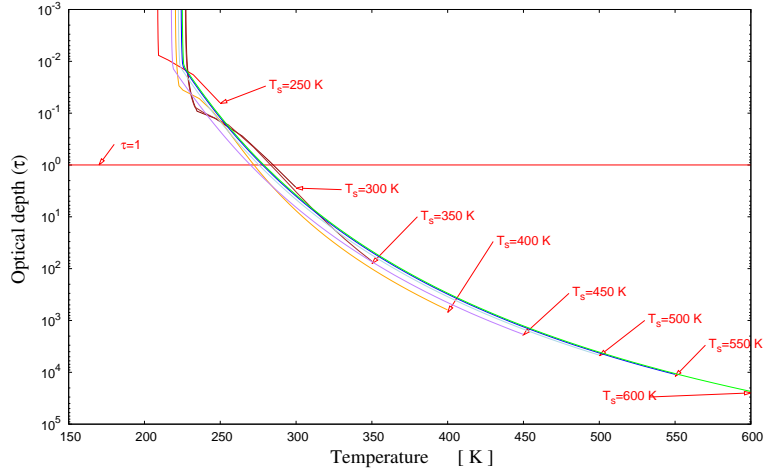


FIG. 13. The relationships between T_s and optical depth (τ) for several T_s cases of $p_{He\ 0} = 10^6\text{ Pa}$ are presented.

The relationships between T_s and optical depth (τ) of $p_{He\ 0} = 10^6\text{ Pa}$ for several T_s cases are presented in Fig. 13. The $T_s = 250\text{K}$, 300K , 350K , 400K , 450K , 500K , 550K , and 600K are presented by red, dark-red, brown, orange, purple, light-blue, blue, and green colour curves, respectively, The unit optical depth ($\tau = 1$) is also presented in red line.

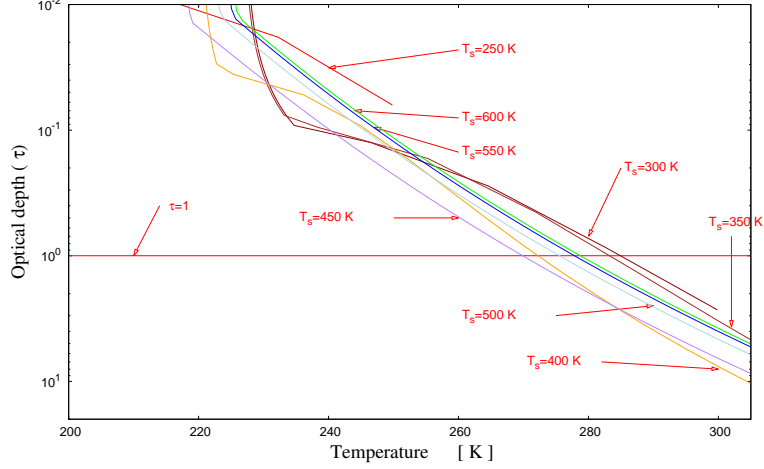


FIG. 14. The relationships between T_s and optical depth (τ) of $p_{He\ 0} = 10^6$ Pa for several T_s cases. It is the magnified figure of Fig. 13.

Fig. 14 is the magnified figure of Fig. 13 to explain the change of F_{IRtop} for different of T_s . The luminosity is mainly radiated at around $\tau \simeq 1$ and the intensity is related to the local temperature of $\tau \simeq 1$. The first bump of $P_{He\ 0} = 10^6$ Pa in Fig. 12 is appeared at $T_s \simeq 300 \sim 350$ K and then the luminosity decreases around $T_s \simeq 400 \sim 450$ K and then increases around $T_s \simeq 500 \sim 600$ K.

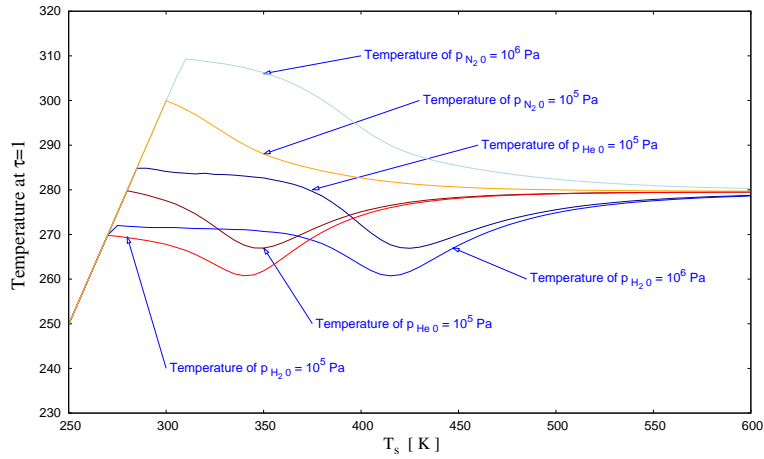


FIG. 15. The relationships between the temperature of UOD (Unity optical depth) and T_s of $p_{He\ 0} = 10^6$ and 10^5 Pa.

The features could be understood in Fig. 15, where the relationship between the temperature at UOD (Unity optical depth) and T_s of $p_{He\ 0} = 10^6$ Pa is presented by dark blue curves. The luminosity decreases around $T_s = 400 \sim 450$ K and then increases around $T_s = 500 \sim 600$ K. The case of $p_{He\ 0} = 10^5$ Pa is shown there by dark red curve. The cases for H₂ atmospheres of $p_{H_2\ 0} = 10^6$ and 10^5 Pa are also presented by blue and red curves, respectively. The cases for N₂ atmospheres of $p_{N_2\ 0} = 10^6$ and 10^5 Pa are also presented for reference by light blue and orange curves, respectively. For the case that the total optical depth is smaller than unity, the temperature of UOD is assumed to be equal to T_s .

In Fig. 16, the relationships between the height of UOD and T_s of $p_{He\ 0} = 10^6$ is presented by dark blue curve. The height of UOD has increased to ~ 250 km, where the temperature of UOD has decreased to ~ 270 K (see Fig. 15). The case of $p_{He\ 0} = 10^5$ Pa is shown there by dark red curve. The cases for H₂ atmospheres of $p_{N_2\ 0} = 10^6$ and 10^5 Pa are also presented by blue and red curves, respectively. The cases for N₂ atmospheres of $p_{N_2\ 0} = 10^6$ and 10^5 Pa are also presented for reference by light blue and orange curves, respectively. The height of UOD is taken to be zero for the case that the total optical depth is smaller than unity.

The relationships between temperature and pressure of $p_{He\ 0} = 10^6$ Pa for several T_s cases are presented in Fig. 17, and the relationships between mole fraction and pressure are shown in Fig. 18. The relationships between mole fraction and optical depth are calculated in Fig. 19.

To compare the cases of N₂, the results of N₂ and He are presented in Fig. 20 for $g=9.8\text{m/s}^2$. The relationships between T_s and F_{IRtop} for several $p_{He\ 0}$ and $p_{N_2\ 0}$ cases are presented there. Several cases of $p_{He\ 0}$ in Fig. 12 are also included here. The case of pure H₂O atmosphere is shown by black curve.

For super-Earth in $g = 9.8 \times 2 \text{ m/s}^2$, it is investigated the gray calculations for cases of background gases with He in Fig 21. The relationships between T_s and F_{IRtop} for several $p_{He\ 0}$ cases are presented. The case of pure H₂O atmosphere is shown by black curve. It is noticed that KI and SN-limits are different from Earth cases in Fig. 12.

It is investigated the gray calculations for cases of background gases with N₂ and He for super-Earth case in Fig. 22. The relationships between T_s and F_{IRtop} for several $p_{N_2\ 0}$ and $p_{He\ 0}$ cases are presented there. Several cases of $p_{He\ 0}$ in Fig. 21 are also included here.

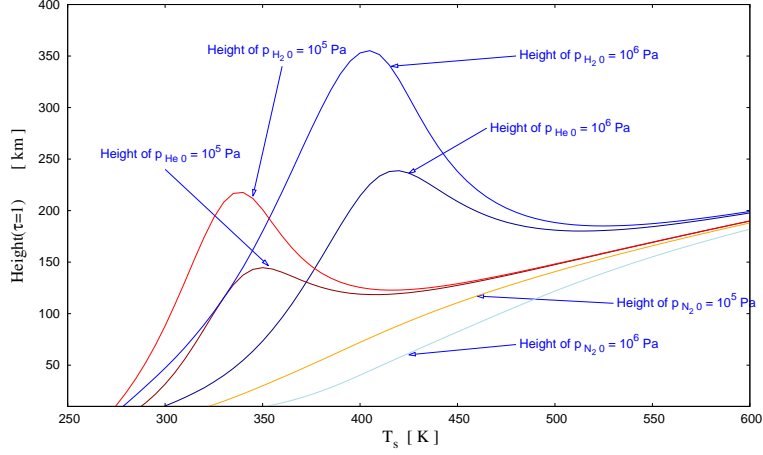


FIG. 16. The relationships between the height of UOD and T_s of $p_{He\ 0} = 10^6$ and 10^5 Pa are presented by dark blue and dark red curves, respectively. The cases for H_2 atmospheres of $p_{H_2\ 0} = 10^6$ and 10^5 Pa and the cases for N_2 atmospheres of $p_{N_2\ 0} = 10^6$ and 10^5 Pa are also presented for reference.

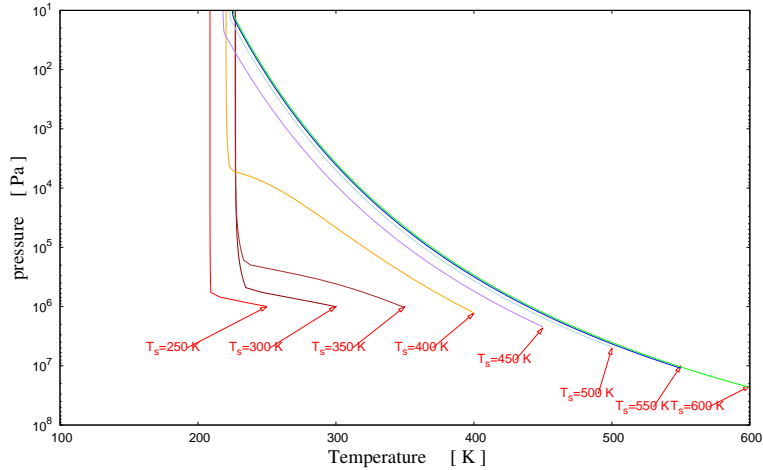


FIG. 17. The relationships between temperature and pressure of $p_{He\ 0} = 10^6$ Pa for several T_s cases with He.

V. KI-LIMIT DEPENDENCE ON THE INITIAL PRESSURE

It is noticed that the KI-limit depends on the initial pressure of the background component as well as MW (molecular weight).

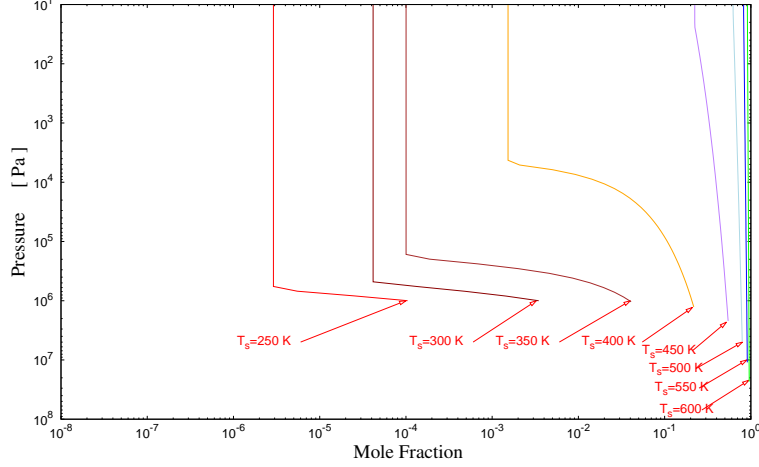


FIG. 18. The relationships between mole fraction and pressure of $p_{He\ 0} = 10^6$ Pa for several T_s cases with He

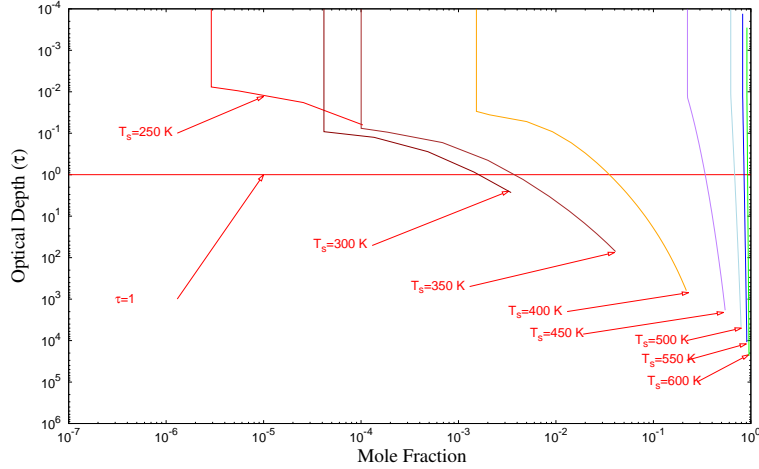


FIG. 19. For He in $g = 9.8m/s^2$, the relationships between mole fraction and optical depth of $p_{He\ 0} = 10^6$ Pa for several T_s cases are presented.

In Fig. 23, the relationship between the optical depth τ_{tp} and the temperature T_{tp} is presented of He atmosphere for $F_{IR\ top}$ as a parameter with 250, 291, and 384 W/m² in $p_{He\ 0} = 10^6$ Pa. The coloured curves represent Eq. (8) for $F_{IR\ top}$ and the almost straight blue curve represents Eq. (9), where the suffix "tp" means the value at the tropopause (Nakajima et al. 1992).

The relationship between T_{tp} and $F_{IR\ top}$ for $p_{He\ 0} = 10^6$ Pa is shown in Fig. 24. The

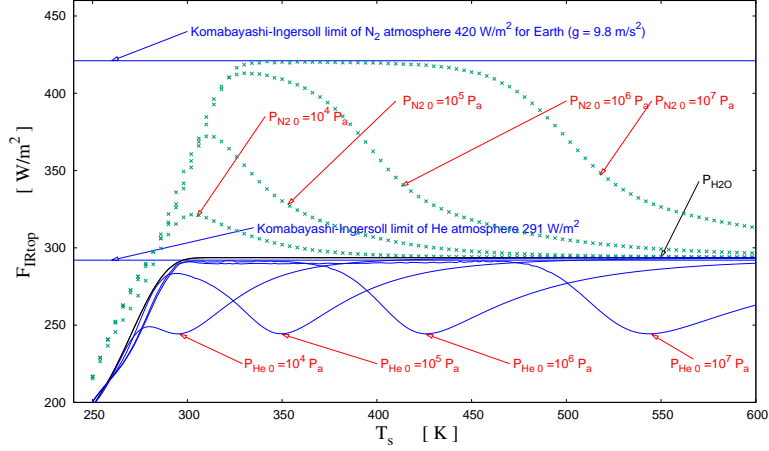


FIG. 20. The relationships between T_s and F_{IRtop} for several $p_{He\ 0}$ and $p_{N_2\ 0}$ cases of background gases with He and N_2 .

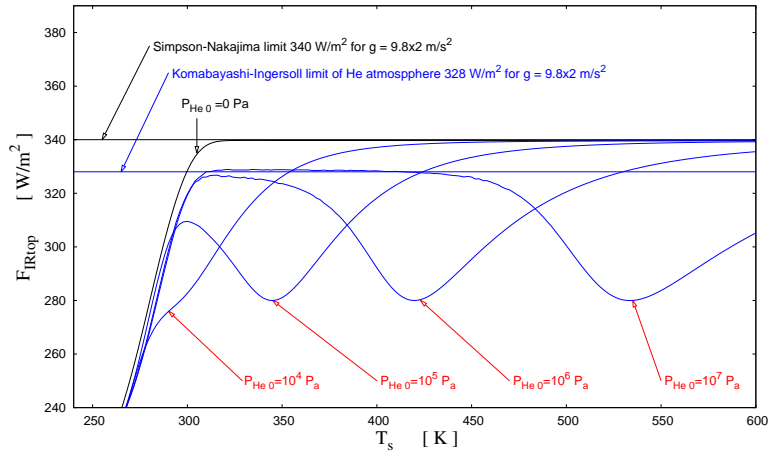


FIG. 21. For super-Earth in $g = 9.8 \times 2 \text{ m/s}^2$, the relationships between T_s and F_{IRtop} for several $p_{He\ 0}$ cases are presented.

KI-limit of this model in He atmosphere is $\simeq 291 \text{ W m}^{-2}$ for $p_{He\ 0} \simeq 10^6 \text{ Pa}$.

In Fig. 25, the relationship between T_{tp} and F_{IRtop} for $p_{He\ 0} = 10^3 \text{ Pa}$ is presented where the KI-limit is $\simeq 298 \text{ W/m}^2$, which is different from $\simeq 291 \text{ W/m}^2$ for $p_{He\ 0} = 10^6 \text{ Pa}$. The KI-limit of He atmosphere is $291 \sim 298 \text{ W/m}^2$ for $p_{He\ 0} \simeq 10^3 \sim 10^6 \text{ Pa}$, which is shown in Fig. 26 as $MW = 4$ case for He. It shows that the KI-limit depends on the initial pressure

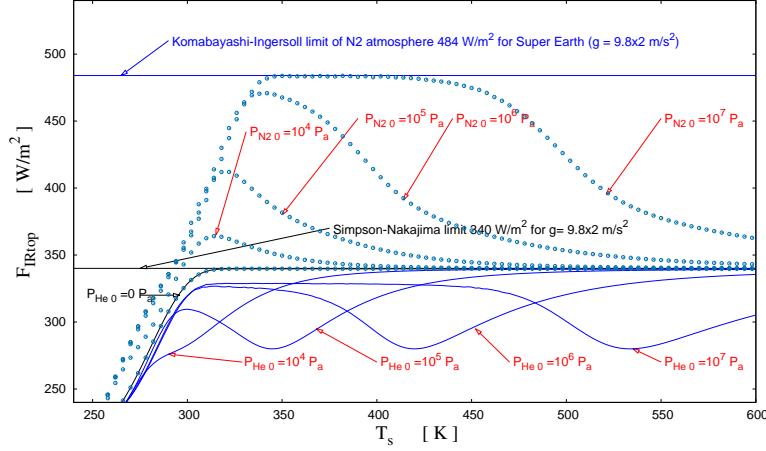


FIG. 22. For super-Earth case of background gases with He and N_2 , the relationships between T_s and F_{IRtop} for several initial $p_{He\ 0}$ and $p_{N_2\ 0}$ cases are presented.

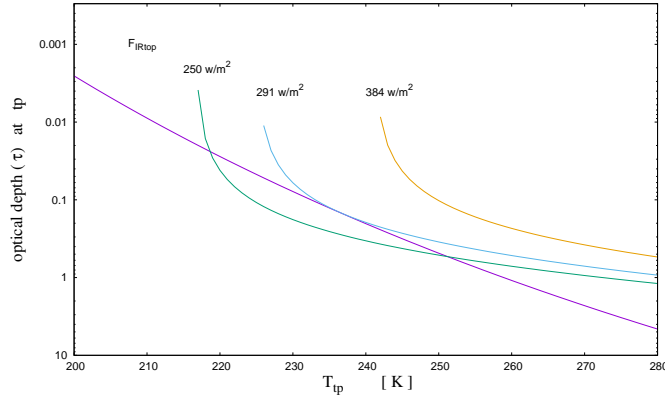


FIG. 23. The relationship between τ_{tp} and T_{tp} of He atmosphere with F_{IRtop} as a parameter for $p_{He\ 0} = 10^6$ Pa.

$p_{He\ 0}$ of the background gas.

In Fig. 26, it is calculated the KI-limit dependence on molecular weight for fixed initial pressure $p_{n\ 0}$ of the background gases. The relationships between molecular weight and F_{IRtop} for each initial pressure of the background gases is presented. For example, in the case that the value of molecular weight is 18 where the molecular weight of every molecule is the same with water H_2O , F_{IRtop} is the same for any initial pressure $p_{n\ 0}$. On the other hand, in the He background atmosphere the mean molecular weight (MMW) for $p_{He\ 0} \simeq 10^{-2} \sim 10^1$

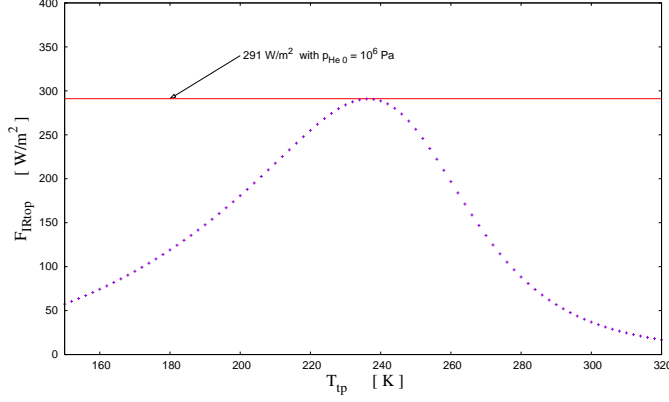


FIG. 24. The relationship between T_{tp} and F_{IRtop} for $p_{He\ 0} = 10^6$ Pa. The KI-limit of this model for He atmosphere is $\simeq 291$ W m $^{-2}$.

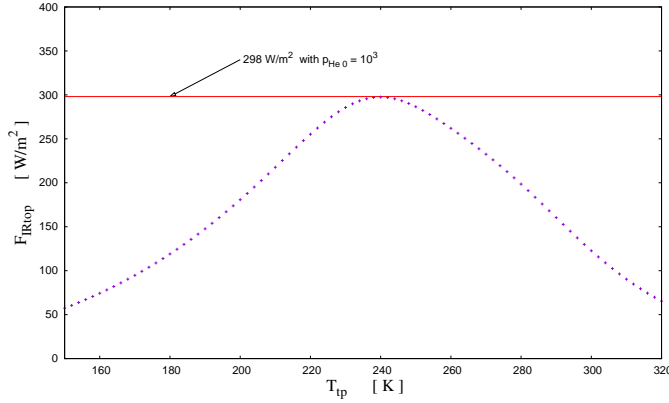


FIG. 25. The relationship between T_s and F_{IRtop} for $p_{He\ 0} \simeq 10^3$ Pa is presented. The KI-limit of this model for He atmosphere is $\simeq 298$ W m $^{-2}$, which is different from $\simeq 291$ W m $^{-2}$ for $p_{He\ 0} \simeq 10^6$ Pa.

Pa, the KI-limit is $\simeq 390$ W/m 2 which is almost the same of $MW = 18$, because the dominant component of the atmosphere is H $_2$ O. For $p_{He\ 0} \simeq 10^4 \sim 10^6$ Pa, KI-limit of $MMW = 4$ is $\simeq 291$ W/m 2 where the dominant component of the atmosphere is He. Even for fixed molecular weight of the background atmosphere, MMW changes due to the increase of H $_2$ O compared to the initial component pressure. The KI-limit depends on the initial component pressure $p_{n\ 0}$.

About the saturation vapour pressure on temperature, we take Eq. (2), so the results in Fig. 26 seem to be independent on any peculiar temperature.

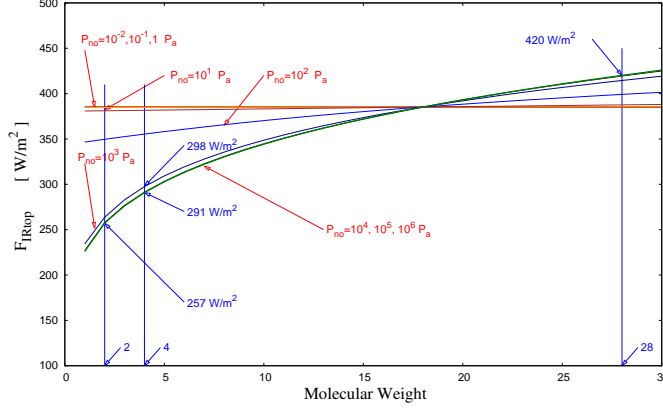


FIG. 26. The KI-limit dependence on molecular weight for fixed initial pressure of the background gases. The relationships between molecular weight and F_{IRtop} for each initial pressure of the background gases is presented. Molecular weight of H_2 , He, and N_2 are shown as 2, 4, and 28, respectively.

VI. RESULTS AND DISCUSSION

We have presented the results of the outgoing radiation for the different components of background gas under a simple model with gray approximation adopted by Nakajima et al. 1992. The main results of the paper are the following:

1. It is studied the possibility of the various atmospheres over oceans.
2. H_2 atmospheres as well as He are investigated. To our concern, the treating He atmosphere in this style seems to be rather new.
3. The strange features are found for H_2 atmosphere as well as He that F_{IRtop} increases to the first upper limit, then decreases and increase again to the second limit : named "Soufflé effect" by Koll & Cronin (2019).
4. The first upper limit is the Komabayashi-Ingersoll limit (KI-limit), which is not stated explicitly by Koll & Cronin (2019).
5. The KI-limit value depends on the molecular weight and the initial pressure of the background atmosphere (Sect. V).
6. The second limit is the Simpson-Nakajima limit (SN-limit) which is the atmosphere mainly composed by vapour, called 'steam limit' (Koll & Cronin 2019).

7. "Soufflé effect" is analysed by taking the UOD (Unit optical depth) temperature which has decreased and the UOD height which has increased.
8. H₂ atmosphere as well as He is the non-condensable background component where the KI-limit is lower than the SN-limit.
9. The mixed gas of the relative realistic mixed atmosphere (H₂ \simeq 72% & He \simeq 28%) is investigated. The first upper limit is $\sim 267\text{W/m}^2$ (Sect. VI).
10. The various approximate limits derived by Koll & Cronin (2019) are investigated and considered its applicability (Appendix B).

From the above consideration, it becomes clear that it must be considered the atmospheric components of the extra terrestrial planets if one want to investigate "Habitable Zone". We would like to expect much more observations further to find out the life trace in extra-terrestrial planets (Hill et al. 2022).

1. *Injection flux vs. Distance from a parent star*

To apply the above results to the planet formation, it is better to consider the solar constant (1364 W/m^2) for Earth orbit where the gravitational acceleration as 9.8m/s^2 . Taking the spherical mean for the injected flux ($\times 1/4$), the flux becomes 341 W/m^2 .

As the solar luminosity is almost 70% of present value at 4.6 Gy ago (Bahcall, Pinsonneault, & Basu 2001), the flux is $\simeq 239\text{ W/m}^2$. If we take the albedo $\simeq 0.3$ which is the corresponding value of Earth at present, the solar injection flux decreases to $\simeq 167\text{ W/m}^2$.

The KI-limit for H₂ atmosphere is $\simeq 257\text{ W/m}^2$ which is greater than the above $\simeq 239\text{ W/m}^2$ and $\simeq 167\text{ W/m}^2$ values. Then it is stable for H₂ atmosphere for assumed planets in Earth orbit. Even for super-Earth, the KI-limit for H₂ atmosphere is $\simeq 295\text{ W/m}^2$ which is greater than the above $\simeq 239\text{ W/m}^2$ and $\simeq 167\text{ W/m}^2$ values. Then it is stable for H₂ atmosphere for assumed super-Earth planets in Earth orbit.

The KI-limit for He atmosphere is $\simeq 291\text{ W/m}^2$ which is greater than the above $\simeq 239\text{ W/m}^2$ and $\simeq 167\text{ W/m}^2$ values. Then it is stable for He atmosphere for the assumed planets in Earth orbit. Even for super-Earth, the KI-limit for He atmosphere is $\simeq 328\text{ W/m}^2$ which is greater than the above $\simeq 239\text{ W/m}^2$ and $\simeq 167\text{ W/m}^2$ values. Then it is stable for He atmosphere for the assumed super-Earth planets in Earth orbit.

If the orbit has decreased to 0.5 Au, the injection flux increased four times as $\simeq 956$ ($=239 \times 4$) W/m^2 and $\simeq 668 \text{ W/m}^2$. Then it becomes unstable for Earth and super-Earth planets, because the situations are over the KI-limit and SN-limit. They will be in a greenhouse runaway and/or moist greenhouse situation.

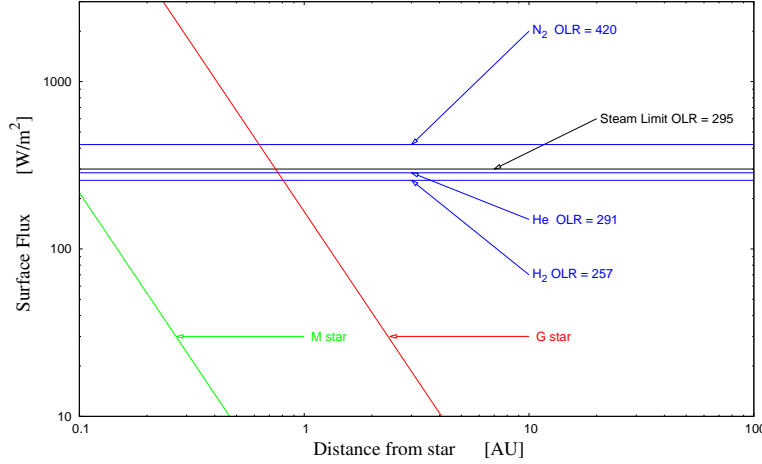


FIG. 27. Injection flux vs. distance from a parent star.

In Fig. 27, the injection flux versus the distance from parent star is shown. The star is taken for a G and an M host star by red and green line, respectively. For an M-type star the luminosity is taken with 1.3 % of the Sun (Pierrehumbert & Gaidos 2011). G star is normalized 167 W/m^2 at 1AU. Three dilute limits for H_2 ($\simeq 257 \text{ W/m}^2$), He ($\simeq 291 \text{ W/m}^2$), and N_2 ($\simeq 420 \text{ W/m}^2$) atmospheres and the steam limit ($\simeq 295 \text{ W/m}^2$) are presented for reference. The steam limit is shown by black.

Under this model, it is found that the OLR upper limit decreases in the H_2 rich atmosphere for the decrease of the mean molecular weight. Then it becomes clear that it is possible to become the runaway situation for super-Earth in the distance smaller than 1AU from the G type star (Sun). Even if OLR has not reached the upper limit, there is a possibility to become dry up the ocean due to the high surface temperature of the greenhouse effect.

If there are extra planets with H_2 atmosphere over ocean and a life such as photosynthetic bacteria of the class Cyanobacteria (indicated by Pierrehumbert & Gaidos, 2011), it must be an unstable situation for the chemical reaction between H_2 and O_2 . It could be a stable

atmosphere with He and O₂. We would like to estimate the diffusion time of H₂ through the initial atmosphere mainly composed H₂ and He (Sekiya, Nakazawa & Hayashi 1980; Wordworth 2012; Hu et al. 2015; Pahlevan et al. 2022).

2. Mixed background gases with H₂ and He

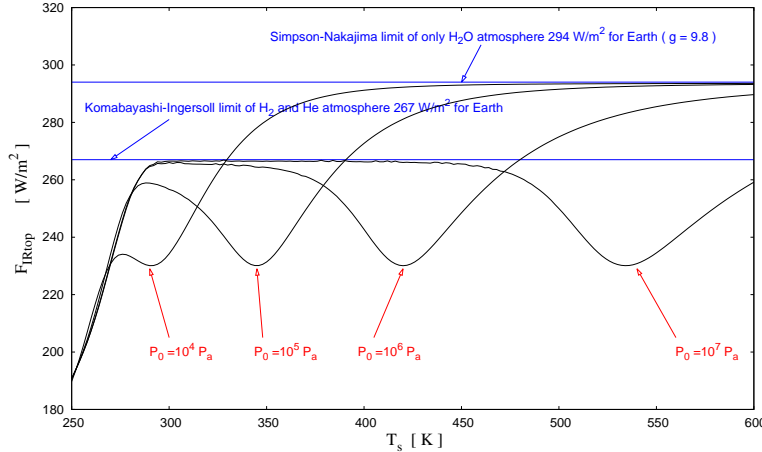


FIG. 28. It is investigated the gray calculations for mixed background gases with H₂ (weight $X \simeq 0.72$) and He (weight $Y \simeq 0.28$) for $g = 9.8 \text{ m/s}^2$.

In Fig. 28, the gray calculations for mixed background gases with H₂ (weight $X \simeq 0.72$) and He (weight $Y \simeq 0.28$) for $g = 9.8 \text{ m/s}^2$ are presented. This mixed gas is considered to be the primordial gas from which Sun and Earth are formed. The relationships between T_s and F_{IRtop} for several initial p_0 ($= 10^4, 10^5, 10^6, \text{ and } 10^7 \text{ Pa}$) cases for Earth are shown. The first upper limit for this atmosphere is $\sim 267 \text{ W/m}^2$, which has increased from H₂ of $\sim 257 \text{ W/m}^2$ (see Fig. 1). The second limit (steam limit) is the same of H₂ and He as $\sim 294 \text{ W/m}^2$.

3. Various uncertainty

There are various uncertainty factors to estimate the relationship between the surface temperature T_s and outgoing infrared radiation at the top of the atmosphere F_{IRtop} . Our results do not apply directly to any real planet history because of large uncertainties in our

calculation due to the absence of clouds and the use of a one-dimensional model. In order to determine quantitatively, it seems to be necessary to evaluate the parameters such as albedo, effects of clouds, and relative humidity, circulation of the atmosphere over the surface of the planet (Manabe & Wetherald 1967, Zsom et al. 2013, Manabe & Broccoli 2020). It will be better to estimate the distribution of those parameters for the greenhouse effects and under the increase of solar luminosity.

a. gray opacity approximation

If one considers more than gray opacity approximation, one has to treat opacity, including the line by line treatments, Lorentz factor, pressure effect, random approximations, and further (Pierrehumbert 2010; Seager 2010), which make the physical understanding to be complicated.

Appendix A: Derivation of the equation (3) in relation to Pierrehumbert (2010)

In this appendix, it is explained that the equation of (4) in Nakajima et al. (1992) (Eq. (3) in this paper) is equivalent to the equation of (2.33) in Pierrehumbert (2010). The notation is followed to Pierrehumbert (2010) and equation number is shown as (Pie. 2.33). As stated before, it is checked for the situation for the different molecular weights of condensible and non-condensable substances (Nakajima et al. have assumed the same for simplicity).

The equation in (Pie. 2.33) is written as

$$\frac{d \ln T}{d \ln p_a} = \frac{R_a}{c_{pa}} \frac{1 + \frac{L}{R_a T} r_{sat}}{1 + \left(\frac{c_{pc}}{c_{pa}} + \left(\frac{L}{R_c T} - 1 \right) \frac{L}{c_{pa} T} \right) r_{sat}}, \quad (\text{A.1})$$

where subscript a and c are related to non-condensable and condensable substance, respectively. Other notations are the following.

A partial pressure of non-condensable substance is described as p_a which is related to total pressure p as $p = p_a + p_c$ where p_c is the partial pressure of condensable substance (water vapour). Then $dp = dp_a + dp_c$. It is introduced saturation assumption that p_c is replaced by $p_{c,sat}$. Using Clausius-Clapeyron to re-write $dp_{c,sat}$ that

$$\frac{dp_{c,sat}}{dT} = \frac{L}{R_c T^2} p_{c,sat}, \quad (\text{A.2})$$

where R_c is the gas constant for the substance which is condensing (water) as shown in (Pie.

2.25) and L is the latent heat associated with the transportation to the more condensed phase.

Then $R_a d \ln p_a$ of the second term in (Pie. 2.32) becomes as

$$R_a d \ln p_a = \frac{R_a}{p_a} \left(dp - \frac{L p_{c,sat} dT}{R_c T^2} \right). \quad (\text{A.3})$$

So the second term in (Pie. 2.32) is written as

$$\begin{aligned} & - \left(1 + \frac{L}{R_a T} r_{sat} \right) \frac{R_a}{p_a} \left(dp - \frac{L p_{c,sat} dT}{R_c T^2} \right) \\ &= - \left(1 + \frac{L}{R_a T} r_{sat} \right) \frac{R_a}{p_a} dp + \left(1 + \frac{L}{R_a T} r_{sat} \right) \frac{R_a}{p_a} \frac{L p_{c,sat}}{R_c T^2} dT. \end{aligned}$$

The term of dT is moved to the first term of (Pie. 2.32).

Then the equation of (Pie. 2.32) becomes for taking $\partial Q = 0$ as

$$\left[\tilde{c}_{pa} + (\tilde{c}_{pc} + \left(\frac{L}{R_c T} - 1 \right) \frac{L}{T}) r_{sat} + \left(1 + \frac{L}{R_a T} r_{sat} \right) \frac{R_a L p_{c,sat}}{p_a R_c T} \right] d \ln T \quad (\text{A.4})$$

$$= \left[\left(1 + \frac{L}{R_a T} r_{sat} \right) \frac{R_a p}{p_a} \right] d \ln p. \quad (\text{A.5})$$

Then taking $r_{sat} = \epsilon p_{c,sat}/p_a$, $\epsilon = M_c/M_a$, $p_a = \rho_a RT/M_a$, $p_c = p_{c,sat} = \rho_c RT/M_c$, $x_n = p_n/p = p_a/p$, and $x_c = p_c/p$, $R_a = R/M_a$, $R_c = R/M_c$, $l = LM_c$, $c_{pa} = \tilde{c}_{pa} M_a$, $c_{pc} = \tilde{c}_{pc} M_c$, where M_a and M_c are molecular weight of the substance a (=n: non-condensable background substance, eg. H₂, He, N₂, and air: suffix 'a' comes from Pierrehumbert and 'n' comes from Nakajima et al.), and c (=v: condensable substance, eg. water vapour), the above equations have changed to the followings.

Using $(R_a L p_c)/(p_a R_c T) = (M_c p_c L)/(M_a p_a T) = (r_{sat} L)/T$, the square bracket of Eq. (A.4) becomes as

$$\begin{aligned} [\dots] &= \left[\tilde{c}_{pa} + \left(\tilde{c}_{pc} + \left(\frac{L}{R_c T} - 1 \right) \frac{L}{T} \right) r_{sat} + \left(1 + \frac{L r_{sat}}{R_a T} \right) \frac{L R_a p_{c,sat}}{p_a R_c T} \right] \\ &= \left[\tilde{c}_{pa} + \left(\tilde{c}_{pc} + \frac{L}{R_c T} \frac{L}{T} \right) r_{sat} - \frac{L}{T} r_{sat} + r_{sat} \frac{L}{T} + \frac{L r_{sat}}{R_a T} \frac{r_{sat} L}{T} \right] \\ &= \left[\tilde{c}_{pa} + \tilde{c}_{pc} r_{sat} + \frac{l^2}{M_c^2} \frac{M_c}{R} \frac{1}{T^2} \frac{M_c}{M_a} \frac{p_c}{p_a} + \frac{l^2 M_a}{M_c^2 R T^2} \frac{M_c^2}{M_a^2} \frac{p_c^2}{p_a^2} \right] \\ &= \frac{1}{M_a} \left[c_{pa} + c_{pc} \frac{x_v}{x_n} + \frac{l^2}{R T^2} \frac{x_v}{x_n} + \frac{l^2}{R T^2} \frac{x_v^2}{x_n^2} \right] \\ &= \frac{c_{pa}}{M_a x_n} \left[x_n + x_v \frac{c_{pc}}{c_{pa}} + \frac{x_v}{x_n} \frac{l^2}{R T^2 c_{pa}} \right], \end{aligned}$$

where we use $x_n + x_c = 1$.

The square bracket of Eq. (A. 5) becomes as

$$\begin{aligned} [\dots] &= \frac{R_a}{x_n} \left[\left(1 + \frac{Lr_{sat}}{R_a T} \right) \right] \\ &= \frac{R_a}{x_n} \left[1 + \frac{l}{RT} \frac{x_c}{x_n} \right]. \end{aligned}$$

Considering $d \ln T / d \ln p = \frac{p}{T} \frac{\partial T}{\partial p}$, the equation (Pie. 2.33) becomes as

$$\left(\frac{\partial T}{\partial p} \right) = \frac{\frac{RT}{pc_{pn}} + \frac{x_v^*}{x_n} \frac{l}{pc_{pn}}}{x_n + x_v^* \frac{c_{pc}}{c_{pn}} + \frac{x_v^*}{x_n} \frac{l^2}{RT^2 c_{pn}}}, \quad (\text{A.6})$$

where we neglect the differences between partial derivative and total derivative, and take $x_c = x_v^*$ and $c_{pa} = c_{pn}$. [1]

Then the derivation of equation (4) in Nakajima et al. is equivalent to the equation of (Pie. 2. 33).

It is also equivalent to the equations of (3.7) and (3.14) in Houghton (1977)

$$dp = -g\rho_a(1 + \xi)dz \quad (\text{A.7})$$

and

$$-\frac{dT}{dz} = \frac{g}{\tilde{c}_{pn}} \frac{(1 + Lp_{c,sat}M_c/pRT)(1 + (p_{c,sat}\epsilon/p))}{1 + (\epsilon p_{c,sat}/p\tilde{c}_{pn})(\tilde{c}_{pc} + (dL/dT) - L/T) + (\epsilon p_{c,sat}L^2M_c/\tilde{c}_{pn}pRT^2)}. \quad (\text{A.8})$$

If the term $dL/dT - L/T$ in the denominator is neglected for its small values, the above two equations becomes equivalent to the equation (3) in this paper and equation of (4) in Nakajima et al. (1992).

Appendix B: Trial to derive the limit values

1. MMW matters (Koll & Cronin 2019)

First, taking the water vapour scale height H_v , $\rho_v = \rho_{v,0}e^{-z/H_v}$, the optical depth is

$$\tau = \int_0^\infty \kappa_v \rho_v dz = \kappa_v \rho_{v,0} \int_0^\infty e^{-z/H_v} dz = \frac{H_v}{l_0}, \quad (\text{B.1})$$

where $l_0 = 1/(\kappa_v \rho_{v,0})$ (in general, the subscript v will denote quantities related to water vapour).

Using the ideal gas law for water vapour, $\rho_v = e^*/(R_v T)$ where e^* is the saturation vapour pressure, and the Clausius-Clapeyron relation, $d \ln e^*/d \ln T = L_v/(R_v T)$ where L_v is the latent heat of vapourization:

$$(-H_v)^{-1} = \frac{1}{\rho_v} \frac{d\rho_v}{dz} = \frac{1}{e^*} \frac{de^*}{dz} - \frac{1}{T} \frac{dT}{dz} = \left(\frac{1}{e^*} \frac{de^*}{dT} - \frac{1}{T} \right) \frac{dT}{dz}, \quad (\text{B.2})$$

and

$$= \left(\frac{L_v}{R_v T} - 1 \right) \frac{1}{T} \frac{dT}{dz} \simeq \frac{L_v}{R_v T} \frac{1}{T} \frac{dT}{dz} = \frac{L_v}{R_v T} H_T^{-1}, \quad (\text{B.3})$$

where $L_v/R_v T \gg 1$ is used.

Here it is denoted $H_T = (-1/T \times dT/dz)^{-1}$ as the temperature scale height, which is related to the water vapour scale height as

$$H_v = \frac{R_v T}{L_v} H_T, \quad (\text{B.4})$$

then it is accepted $H_T \gg H_v$ for water vapour and a wide range of other condensible gases.

In the low temperature limit, the lapse rate is assumed to be the dry adiabat, $dT/dz = -g/c_p$, and

$$H_T^{dilute} = \frac{c_p T}{g}. \quad (\text{B.5})$$

At high temperature the total pressure is dominated by the saturation vapour pressure of water and the temperature scale height is given by

$$H_T^{steam} = -T \frac{dz}{dT} = -T \frac{dz}{de^*} \frac{de^*}{dT} = T \frac{1}{\rho_v g} \frac{L_v e^*}{R_v T^2} = \frac{L_v}{g}, \quad (\text{B.6})$$

where the hydrostatic equation, $de^*/dz = -\rho_v g$, is used.

It should be noted that at a temperature of 400 K with an Earth-like gravity, $H_T^{dilute} \simeq 350$ km in H_2 , whereas $H_T^{dilute} \simeq 40$ km in N_2 . The main difference is due to the low molecular weight of H_2 relative to N_2 (see Fig. 5).

2. Trial to derive the steam and dilute limit values

Koll & Cronin (2019) have tried to derive an approximate analytical expression for the OLR limit values of the steam limit (SN-limit) and dilute limit (KI-limit). They have approximated the saturation pressure with temperature as

$$p^*(T) = p_0^* \left(\frac{T}{T_0} \right)^\gamma, \quad (\text{B.7})$$

taking the Clausius-Clapeyron relation $d \ln p^*/d \ln T \simeq L_v/(R_v T) = \gamma$. They have expressed the relation between optical depth and temperature as a power law (see Koll & Cronin 2019)

$$\tau(T) = \kappa H_T \frac{p_0^*}{L_v} \times \left(\frac{T}{T_0} \right)^\gamma, \quad (\text{B.8})$$

where T_0 is a reference temperature close to the interest range.

OLR is said to be equal to

$$\text{OLR} = \sigma T_s^4 e^{-\tau} + \int_0^\tau \sigma T(\tau')^4 e^{-\tau'} d\tau', \quad (\text{B.9})$$

the first term can be neglected as optical depth increasing and the upper limit of the integral is replaced with infinity

$$\text{OLR}_\infty \simeq \int_0^\infty \sigma T(\tau)^4 e^{-\tau} d\tau, \quad (\text{B.10})$$

$$= \sigma T_0^4 \int_0^\infty \left(\frac{\tau}{\tau_0} \right)^{4/\gamma} e^{-\tau} d\tau, \quad (\text{B.11})$$

$$= \sigma T_0^4 \tau_0^{-4/\gamma} \int_0^\infty \tau^{4/\gamma} e^{-\tau} d\tau, \quad (\text{B.12})$$

$$\text{OLR}_\infty \simeq \sigma T_0^4 \times \frac{\Gamma(1 + 4/\gamma)}{\tau_0^{4/\gamma}}. \quad (\text{B.13})$$

Here Γ is the gamma function, defined by $\Gamma(s) = \int_0^\infty x^{s-1} \exp(-x) dx$, and τ_0 denotes for steam limit

$$\tau_0 = \frac{\kappa_v p^*(T_0)}{g}, \quad (\text{B.14})$$

and for dilute limit

$$\tau_0 = \frac{\kappa_v p^*(T_0) c_p T_0}{g L_v}, \quad (\text{B.15})$$

where it is taken $c_p = 7R/2$ for H_2 and N_2 diatomic molecule and $c_p = 5R/2$ for He monoatomic molecule. The latent heat L_v is tentatively taken, for the moment, as $2265 - 4.186 \times (T_0 - 373)$ (J/g), where 2265 (J/g) is the vapourization energy per gram at 373K and 4.186 (J/(g·K)) is the specific heat of water, approximately.

Dilute limit dependence on T_0 for H_2 , He, and N_2 atmospheres given by Eqs. (B.13) and (B.15) are presented by blue, green, and orange curve in Fig. 29, respectively. For the steam

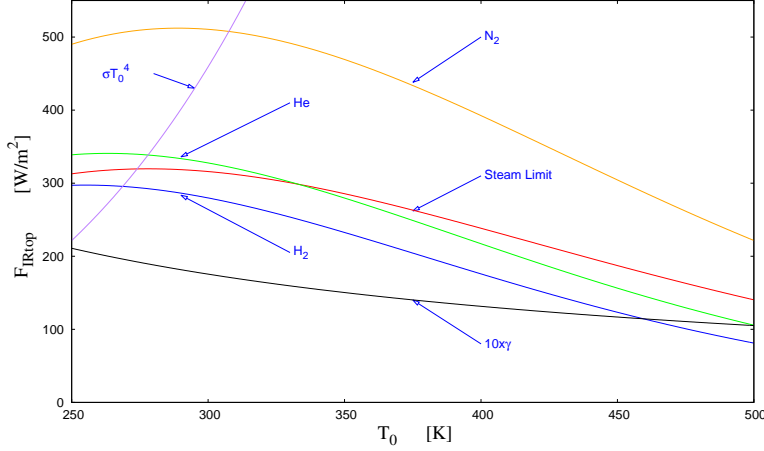


FIG. 29. Dilute limit dependence on T_0 for H_2 , He , and N_2 atmospheres given by Eqs. (B.13) and (B.15) are presented.

limit given by Eqs. (B.13) and (B.14) is presented by red curve in Fig. 29. They are almost constant or monotonically decreasing with T_0 , however the value of σT_0^4 has changed which is shown for reference by purple curve in Fig. 29.

Taking $T_1 = T_0 - \Delta T$ and $T_2 = T_0 + \Delta T$, γ for T_0 is taken as a mean value of γ_i as $(\gamma_1 + \gamma_2)/2$ where

$$\gamma_i = \frac{L}{R} \times \left(\frac{1/T_i - 1/T_0}{\ln T_0 - \ln T_i} \right), \quad (\text{B.16})$$

being i ($=1, 2$) and $\Delta = 25$. Ten times of γ is presented in Fig. 29 in black curve as $10 \times \gamma$ and some γ values are shown in Table I.

It must be noticed that He dilute limit (green line) lies below the steam limit (red line) beyond $T_0 \simeq 330$ K, which is not indicated by Koll & Cronin 2019.

For taking $T_0 \simeq 300$ K where $\gamma \simeq 17.55$, $OLR \simeq 316$ W/m^2 for steam limit (calculated result is $\simeq 294$ W/m^2 (Fig. 1); then $316/294 \simeq 1.075$: the difference is $\simeq 7.5\%$). The dilute limit of H_2 atmosphere is $\simeq 280$ W/m^2 (calculated result is $\simeq 257$ W/m^2 (Fig. 1), then $280/257 \simeq 1.089$: the difference is $\simeq 8.9\%$). The dilute limit of He atmosphere is $\simeq 328$ W/m^2 (calculated result is $\simeq 291$ W/m^2 (Fig. 12), then $328/291 \simeq 1.127$: the difference is $\simeq 13\%$). The dilute limit of N_2 atmosphere is $\simeq 511$ W/m^2 (calculated result is $\simeq 420$ W/m^2 (Fig. 9), then $511/420 \simeq 1.217$: the difference is $\simeq 22\%$).

Although they have shown some limiting values, it seems to be a little bit difficult to

accept that the limiting values could approximately represent the calculated values. The absolute limiting values seems to have some differences (dilute limit of N_2 differs about 22 %) for $T_0 \simeq 300K$ and (dilute limit of H_2 is only about 32 % (differs 68 %) for $T_0 \simeq 500K$. They are shown in Fig. 29 and particular values are presented in Table I.

Let us consider the limiting values from the different point. The relative differences of the limiting values could be understood by the above Eq. (B.14).

1. The difference of the accelerating gravity: if g has changed to αg by factor α , τ_0 has changed to τ_0/α and OLR_∞ has changed by factor $\alpha^{4/\gamma}$. Taking $\alpha = 2$ and $\gamma \simeq 17.55$, it becomes $2^{0.2279} \simeq 1.1711$. The steam limit has changed from $\simeq 294 \text{ W/m}^2$ (Fig. 1) to $\simeq 340 \text{ W/m}^2$ (Fig. 10) which is almost the same as $340/294 \simeq 1.1564(1.1711/1.1564 \simeq 1.0128)$. The difference is within 1.3%. . The dilute limit for H_2 , it has changed from $\simeq 257 \text{ W/m}^2$ (Fig. 1) to $\simeq 295 \text{ W/m}^2$ (Fig. 10) where $295/257 \simeq 1.1479$ ($1.1711/1.1479 \simeq 1.0202$). The difference is within 2.1 %. The dilute limit for He , it has changed from $\simeq 291 \text{ W/m}^2$ (Fig. 12) to $\simeq 328 \text{ W/m}^2$ (Fig. 21) where $328/291 \simeq 1.12714$ ($1.1711/1.2714 \simeq 0.9211$). The difference is within 7.9 %. The dilute limit for N_2 , it has changed from $\simeq 420 \text{ W/m}^2$ (Fig. 9) to $\simeq 484 \text{ W/m}^2$ (Fig. 22) where $480/420 \simeq 1.14286$ ($1.1711/1.14286 \simeq 1.0247$). The difference is within 2.5 %.

2. The difference of the mean molecular weight: c_p is the specific heat per gram related to the specific heat per mol $\hat{c}_p = c_p \times MW$ where MW is the molecular weight. Then if the molecular weight has increased by factor β , τ_0 has decreased by factor β . The τ_0 has changed to τ_0/β and OLR_∞ has changed by factor $\beta^{4/\gamma}$. Taking $\beta = 2$ from H_2 to He and $\gamma \simeq 17.55$, it becomes $2^{0.22792} \simeq 1.1711$. The dilute limit has changed from $\simeq 257 \text{ W/m}^2$ (Fig. 1) to $\simeq 291 \text{ W/m}^2$ (Fig. 12) which is almost the same as $291/257 \simeq 1.132(1.1711/1.1323 \simeq 1.0343)$. The difference is within 3.5 %.

Taking $\beta = 14$ from H_2 to N_2 and $\gamma \simeq 17.55$, it becomes $14^{0.22792} \simeq 1.8248$. The dilute limit has changed from $\simeq 257 \text{ W/m}^2$ (Fig. 1) to $\simeq 420 \text{ W/m}^2$ (Fig. 9) which is almost the same as $420/257 \simeq 1.63424(1.8248/1.63424 \simeq 1.117)$. The difference is within 12 %.

Taking $\beta = 7$ from He to N_2 and $\gamma \simeq 17.55$, it becomes $7^{0.222792} \simeq 1.5582$. The dilute limit has changed from $\simeq 291 \text{ W/m}^2$ (Fig. 12) to $\simeq 420 \text{ W/m}^2$ (Fig. 9) which is almost the same as $420/291 \simeq 1.4433(1.5582/1.4433 \simeq 1.0796)$. The difference is within 8.0 %.

It is a rather good approximation to estimate the OLR_∞ by the variation of gravity (differences are within 7.9 %) and molecular weight (differences are within 12 %).

TABLE I. Values of γ , the steam limit (SL), dilute limit of H₂, He and N₂ for T₀ are presented. R1, R2, R3 and R4 show the ratio of the approximate value to the calculated value.

T ₀ K	γ	SL	R1	H ₂	R2	He	R3	N ₂	R4
300	17.55	316	1.078	280	1.089	328	1.126	511	1.216
350	15.03	286	0.975	233	0.905	280	0.961	469	1.117
400	13.15	238	0.813	176	0.684	217	0.746	393	0.935
450	11.68	187	0.639	123	0.480	156	0.537	304	0.725
500	10.51	140	0.479	81.2	0.316	106	0.363	222	0.528

In the Table I the particular values of γ , the steam limit and the dilute limit for of H₂, He and N₂ are shown, where SL, H₂, He and N₂ represent steam limit, dilute limit of H₂, He and N₂, respectively. R1, R2, R3 and R4 show the ratio of the approximate value to the calculated value, as SL/293, H₂/257, He/ 291 and N₂/420, respectively. For example in T₀ \simeq 300 K, the difference of the steam limit is \simeq 7.8 %. The difference of the dilute limit of H₂ is \simeq 8.9 %. If T₀ has changed to 500 K, the differences have increased much further.

From the values in the Table I, the approximate analytical expressions seems to be applicable in the temperature T₀ \simeq 300 \sim 350 K where the differences are within and around 20 % (not bad). For T₀ \geq 400 K, the differences are worse than 20 %. The reason is not so clear for the moment.

Appendix C: Try to derive Eq. (33) in Koll & Cronin (2019)

We have tried to derive the following three equations in Koll & Cronin (2019),

$$\frac{dp}{dz}|_{steam} = -\bar{\rho}g, \quad (\text{KC 32})$$

$$\approx \rho_\nu g \times \left(1 + \frac{R_d - R_\nu p_d}{R_d e^*}\right), \quad (\text{KC 33})$$

$$H_T = \frac{L_\nu}{g} \left(1 + \frac{R_d - R_\nu p_d}{R_d e^*}\right), \quad (\text{KC 34})$$

where (KC 32) represents Eq. (32) in Koll & Cronin (2019) and so on.

Using $p = p_\nu + p_d = e^* + p_d$ and $x_d = p_d/p$, the equation of (KC 32) becomes

$$\frac{dp}{dz}|_{steam} = \frac{dp}{dz} - \frac{dp_d}{dz} \approx -(\rho_\nu + \rho_d)g + (\rho_\nu + \rho_d)x_d g$$

$$\begin{aligned}
&= -\rho_\nu g(1 - x_d) \left(1 + \frac{\rho_d}{\rho_\nu}\right) = -\rho_\nu g \left(1 - \frac{1}{1 + p_d/e^*} \frac{p_d}{e^*}\right) \left(1 + \frac{p_d}{e^*} \frac{R_\nu}{R_d}\right) \\
&\approx -\rho_\nu g \left(1 + \left(\frac{R_\nu}{R_d} - \frac{1}{1 + p_d/e^*}\right) \frac{p_d}{e^*}\right) \\
&\approx -\rho_\nu g \left(1 + \left(\frac{R_\nu - R_d}{R_d}\right) \frac{p_d}{e^*}\right),
\end{aligned}$$

where we use the relation $p_\nu = e^* = \rho_\nu R_\nu T$, $p_d = e^* = \rho_d R_d T$, and $p_d/e^* \ll 1$. It must be noticed that signatures in and out of the parentheses are different from (KC 33). We believe that those are typos.

Using the Clausius-Clapeyron relation, $d \ln e^*/d \ln T = L_\nu/(R_\nu T)$, Eq. (KC 34) becomes as

$$\begin{aligned}
H_T &= -T \frac{dz}{dp} \frac{dp}{dT} \approx -T \frac{dz}{de^*} \frac{de^*}{dT} \approx -\frac{T}{\rho_\nu g} \left(1 + \frac{R_\nu - R_d}{R_d} \frac{p_d}{e^*}\right)^{(-1)} \frac{L_\nu e^*}{R_\nu T^2} \\
&\approx \frac{L_\nu}{g} \left(1 - \frac{R_\nu - R_d}{R_d} \frac{p_d}{e^*}\right) = \frac{L_\nu}{g} \left(1 + \frac{R_d - R_\nu}{R_d} \frac{p_d}{e^*}\right).
\end{aligned}$$

where it must be noticed that the signature of the term in the parenthesis is exact of Eq. (KC 34).

[1]

When the altitude rises above the sea level and the pressure drops, the liquid precipitates, but since the liquid does little work, the approximation here is to omit the contribution of the liquid from the system. Therefore, since the reversibility is lost from the equation $dS = 0$, it is described as quasiadiabat.

Betts, H. C., Puttick, M. N., Clark, J. W., et al. 2018, *Nature Ecology & Evolution*, 2, 1556,

Bressler, S., & Shaviv, G., 2015, *Astronomical Rev.* 11, 41.

Goldblatt C., Robinson T.D., Zahnle K. J., & Crisp D. 2013, *Nature Geosci.* 6, 661.

Goldblatt C., & Watson A. J. 2012, *Phil. Trans. R. Soc.* A370, 4197.

Hara T., & Suzuki A. 2021, *SCIREA J. Physics*, 6, 154, (<https://doi.org/10.54647/physics14381>;
arXiv: 2009.04040),

Hill L. M., Bott K., Dalba A. P., Fetherolf T., Kane R. S., Kopparapu R., Li Z., & Osberg C.

2022, arXiv:2210.02484v1.

Houghton J. T. 1977, *The Physics of Atmospheres*, Cambridge Univ. Press, Cambridge, UK.

Hu R., Seager S., & Yung Y. L. 2015, *ApJ*, 807, 8.

Ingersoll A. P. 1969, *J. Atmos. Sci.* 26, 1191.

Kasting J.F. 1988, *Icarus*, 74, 472.

Koll D.D.B., & Cronin T. W. 2019, *ApJ*. 881,120.

Komabayashi M. 1967, *J. Meteor. Soc. Japan*, 45, 137.

Madhusudhan N., Piette A.A.A., & Constantinou S. 2021, arXiv:2108.10888v2.

Manabe S., & Broccoli A. J. 2020, *Beyond Global Warming: How Numerical Models Revealed the Secrets of Climate Change*, Princeton Univ. Press, Princeton, NJ.

Manabe S., & Wetherald R.T. 1967, *J. Atmos. Sci.*, 24, 241.

Nakajima S., Hayashi Y., & Abe Y. 1992, *J. Atmospheric. Scie.* 23, 2256.

Pahlevan K, Schaefer L., Elkins-Tanton L., Desch J. S, & Buseck R. P. 2022. arXiv: 2209.10635.

Pierrehumbert R.T. 2010, *Exoplanet Atmosphere: Physical Process*, Cambridge Univ. Press, Cambridge, UK.

Pierrehumbert R., & Gaidos, E. 2011, *ApJ*, 734, L13.

Seager S. 2010, *Exoplanet Atmosphere: Physical Process*, Princeton Univ. Press, Princeton, NJ.

Sekiya M., Nakazawa K., & Hayashi C. 1980, *EPSL*, 50, 197.

Sekiya M., Nakazawa K., & Hayashi C. 1981, *Prog. Theor. Phys.* 66, 1301.

Simpson, G. C. 1927, *Mem. R. Meteorol. Soc.* 11, 69.

Suzuki A. Part of the work was postered at Quy Nhon, Vietnam (Dec. 11-17, 2016). 2017, Master thesis at Kyoto Sangyo University in Japanese.

Wordsworth R., 2012, *Icar*, 219, 267.

Wordsworth R., Pierrehumbert R., & Del Genio A.D. 2013, *Science* 339, Issue 6115, 64.

Zsom A., Seager S., de Witt J., & Stamenkovic V. 2013, *ApJ*, 778, 109.